THE JOURNAL OF BIOLOGICAL CHEMISTRY
Vol. 280, No. 19, Issue of May 13, pp. 18908–18915, 2005
Printed in U.S.A.

Structure of the Complex between Plastocyanin and Cytochrome *f* from the Cyanobacterium *Nostoc* sp. PCC 7119 as Determined by Paramagnetic NMR

THE BALANCE BETWEEN ELECTROSTATIC AND HYDROPHOBIC INTERACTIONS WITHIN THE TRANSIENT COMPLEX DETERMINES THE RELATIVE ORIENTATION OF THE TWO PROTEINS*[S]

Received for publication, November 25, 2004, and in revised form, February 3, 2005
Published, JBC Papers in Press, February 10, 2005, DOI 10.1074/jbc.M413298200

Irene Díaz-Moreno‡§, Antonio Díaz-Quintana‡, Miguel A. De la Rosa‡, and Marcellus Ubbink§¶

From the ‡Instituto de Bioquímica Vegetal y Fotosíntesis, Universidad de Sevilla y Consejo Superior de Investigaciones Científicas, Avda. Américo Vespucio 49, 41092 Sevilla, Spain, and §Leiden Institute of Chemistry, Leiden University, Gorlaeus Laboratories, P. O. Box 9502, 2300 RA Leiden, The Netherlands

The complex between cytochrome *f* and plastocyanin from the cyanobacterium *Nostoc* has been characterized by NMR spectroscopy. The binding constant is 16 mM^{-1}, and the lifetime of the complex is much less than 10 ms. Intermolecular pseudo-contact shifts observed for the plastocyanin amide nuclei, caused by the heme iron, as well as the chemical-shift perturbation data were used as the sole experimental restraints to determine the orientation of plastocyanin relative to cytochrome *f* with a precision of 1.3 Å. The data show that the hydrophobic patch surrounding tyrosine 1 in cytochrome *f* docks the hydrophobic patch of plastocyanin. Charge complementarities are found between the rims of the respective recognition sites of cytochrome *f* and plastocyanin. Significant differences in the relative orientation of both proteins are found between this complex and those previously reported for plants and *Phormidium*, indicating that electrostatic and hydrophobic interactions are balanced differently in these complexes.

In oxygen-evolving photosynthetic organisms, light-driven ATP synthesis requires the participation of cytochrome b_6f complex (1, 2), which couples proton translocation across the thylakoid membrane to the electron transport between PSI[1] and PSII (3). In the cytochrome b_6f complex, cytochrome *f* (C*f*) transfers electrons from the Rieske iron sulfur cluster to a soluble metalloprotein that acts as the electron donor for the P700 cofactor of PSI. The C*f* subunit consists of a ~28-kDa N-terminal soluble part anchored to the membrane by a C-terminal helix (4). It represents an atypical *c*-type cytochrome because of both its β-sheet secondary structure and the unusual heme axial coordination (5). The long axis of the soluble part is tilted relative to the membrane normal, and the heme is oriented appropriately for approach of the Rieske protein from the membrane side and of plastocyanin (Pc) from the luminal side (6, 7).

Pc is the most ubiquitous electron carrier between C*f* and P700 (8). It is a type I cupredoxin (9) that consists of an anti-parallel β-sandwich structure with a single copper atom (10–12) that is coordinated by two nitrogen atoms and two sulfur atoms from highly conserved residues.

In addition to its physiological relevance, the electron transfer reaction between C*f* and Pc represents an excellent case to study the transient nature of protein interactions in electron transfer chains (13). The lifetime of this kind of complexes is on the order of 1 ms or less. Due to the large amount of functional data available, this reaction has become a very useful model to test theoretical approaches for the prediction of structures of protein-protein complexes (14–20).

In plants this reaction shows fast kinetics at 100 mM ionic strength ($>10^8$ M^{-1} s^{-1}) despite both its modest binding constant (~7 mM^{-1}) under these conditions and the small difference in redox potential (20 mV) between donor and acceptor (21, 22). The mechanism of this electron transfer reaction has been studied with several techniques (22). Such studies support the importance of electrostatic interactions involving the acidic patches ("site 2") on Pc and the basic residues of C*f* for binding under *in vitro* conditions (23–26) and the essential role of specific residues in the hydrophobic patches of both C*f* (27) and Pc (26). Notably, the relevance of the electrostatic interactions could not be confirmed *in vivo* (15). In the system from *Phormidium laminosum*, the only cyanobacterium for which the kinetics of the reduction reaction have been analyzed so far, the electrostatic effects appear to be weaker and less optimized compared with plants (28, 29).

The solution structures of two Pc-C*f* complexes have been obtained by dissecting the diamagnetic and paramagnetic contributions to the chemical-shift perturbations of Pc resonances upon C*f* binding. The first one (PDB entry 2PCF) corresponds to the complex between spinach Pc and turnip C*f* (30), and the second corresponds to the proteins from *P. laminosum* (31). Both structures show modest interface areas (600–850 $Å^2$ per protein). Moreover, in both cases the hydrophobic patch of Pc

* This work was supported by Program Human Potential and Mobility of Researchers of the European Commission Contract HPRN-CT-1999-00095 "Transient Network," Spanish Ministry of Education, Culture, and Sport Grant AP2000-2937, Spanish Ministry of Science and Technology Grant BMC2003-00458, the Andalusian Government Grant CVI-0198, and Netherlands Organization for Scientific Research Grant 700.52.425. The costs of publication of this article were defrayed in part by the payment of page charges. This article must therefore be hereby marked "*advertisement*" in accordance with 18 U.S.C. Section 1734 solely to indicate this fact.

[S] The on-line version of this article (available at http://www.jbc.org) contains supplemental material.

The atomic coordinates and structure factors (code 1TU2) have been deposited in the Protein Data Bank, Research Collaboratory for Structural Bioinformatics, Rutgers University, New Brunswick, NJ (http://www.rcsb.org/).

¶ To whom correspondence should be addressed. Tel.: 31-71-527-4628; Fax: 31-71-527-4349; E-mail: m.ubbink@chem.leidenuniv.nl.

[1] The abbreviations used are: PSI, photosystem I; PSII, photosystem II; C*f*, water-soluble fragment of cytochrome *f*; HSQC, heteronuclear single-quantum coherence; Pc, plastocyanin; PCd, cadmium plastocyanin; PCS, pseudo-contact shifts; r.m.s.d., root mean square deviation; WT, wild type.

("site 1") lies near Tyr-1 of C*f*, thus providing an appropriate environment for efficient electron transfer toward the copper atom through the exposed copper-coordinating His residue. In addition to this, chemical-shift perturbation data have been reported for several heterologous plant and cyanobacterial systems (32–34). Despite their similarities, significant differences are found between the cyanobacterial and the plant complexes. In *Phormidium*, Pc binds C*f* in a "head-on" conformation in which the hydrophobic patch accounts for the whole recognition interface in Pc, contrary to the "side-on" interface that also involves the acidic patches, which is found in the plant complex. Both kinds of complexes have been predicted in theoretical studies using the co-ordinates from plant proteins (15–17). The ionic strength dependences of the structures suggest that in the plant complex electrostatics play a dominant role, whereas in *Phormidium* complex formation is governed by the hydrophobic effect.

It is known that *Phormidium* is a thermophilic organism (35). A higher ambient temperature could influence the balance between electrostatic forces and hydrophobic effects, making this complex unusual and different from that in other cyanobacteria. Hence, it is unknown if differences between the reported plant and *Phormidium* complexes are applicable to all cyanobacteria. Here, the structure of the complex between Pc and C*f* from another cyanobacterium, *Nostoc* (formerly *Anabaena*), has been determined. Interestingly, the results herein presented are consistent with a single conformation in the transient complex between Pc and C*f* that resembles the characteristic side-on binding mode present in plants yet has an interface similar to that found in the *Phormidium* complex.

EXPERIMENTAL PROCEDURES

Protein Preparation—Uniformly (99%) ^{15}N-labeled *Nostoc* sp. PCC 7119 Pc was produced in *Escherichia coli* JM109 transformed with pEAP-WT (36). The culture conditions and purification methods will be published elsewhere (64). Cadmium substitution of the copper in plastocyanin was performed as published (37) except that a PD-10 column (Amersham Biosciences) pre-equilibrated with a solution of 50 mM HEPES, pH 7.0, containing 1 mM $CdCl_2$ was used instead of a Sephadex G25 gel filtration column.

The soluble part of *Nostoc* sp. PCC 7119 C*f* was produced in *E. coli* DH5α transformed with both pEC86, containing the *c*-type cytochrome maturation cassette (38), and an expression vector for C*f*, pEAF-WT, obtained by insertion of a chimeric *pet*A gene in pBluescript II (Stratagene). This chimeric gene coded for a fusion protein with C*f* truncated at the C terminus (at position 253) and the signal peptide of cytochrome c_6 (36). Cells were grown in LB medium with 100 μg/ml ampicillin, 12 μg/ml chloramphenicol, and 6 mg/ml $Fe(NH_4)_3$ citrate under semi-anaerobic conditions (39) at 35.5 °C, 150 rpm for 32 h up to an A_{600} of 1.3. Protein yields up to 1.5 mg/liter were obtained in this manner. The purification procedure used for C*f* expressed from pEAF-WT will be described elsewhere.[2]

NMR Sample Preparation—Pc and PCd protein solutions were concentrated to the required volume by ultrafiltration methods (Amicon, YM3 membrane) and exchanged into 10 mM sodium phosphate, pH 6.0, H_2O/D_2O 95:5 solutions. Protein concentrations were determined by absorption spectrophotometry using a ϵ_{598} of 4.5 mM^{-1} cm^{-1} for the oxidized form of Pc and a ϵ_{278} of 5.5 mM^{-1} cm^{-1} for PCd. The PCd ϵ_{278} was estimated using protein concentration values from Bradford assays. A A_{278}/A_{598} ratio of 1.0 of the oxidized Pc indicated sufficient purity for characterization by NMR. The stock concentrations were 2.0 mM ^{15}N-labeled Pc and 2.7 mM ^{15}N-labeled PCd.

The soluble domain of C*f* was concentrated using Amicon YM10 membrane and exchanged into 10 mM sodium phosphate, pH 6.0, 3 mM sodium ascorbate, H_2O/D_2O 95:5 solutions. The concentration determination was based on optical spectroscopy using an ϵ_{556} of 31.5 mM^{-1} cm^{-1} for the reduced C*f* (30). A 3.7 mM ferrous C*f* stock solution with a A_{278}/A_{598} ratio of 0.9 was used. C*f* was kept in a reduced form with a few equivalents of sodium ascorbate and was stable in this form for days. The ferric form was prepared by the addition of a 5-fold excess of potassium ferricyanide ($K_3[Fe(CN)_6]$) followed by gel filtration (Amersham Biosciences Superdex G75) to remove ferrocyanide. Complete oxidation was verified by the disappearance of the absorption band at 556 nm. Then, a 2.0 mM ferric C*f* stock solution was prepared.

NMR Spectroscopy—All NMR experiments were performed on a Bruker DMX 600 NMR spectrometer operating at 298 K. The ^{1}H and ^{15}N assignments of reduced *Nostoc* Pc assignments were taken from Badsberg *et al.* (40). For sequence-specific assignment of the backbone amide resonances of PCd (Supplemental Table S2), a two-dimensional ^{1}H,^{15}N HSQC (41), two-dimensional ^{1}H,^{15}N HSQC nuclear Overhauser enhancement spectroscopy with 150 ms mixing time, and two-dimensional ^{1}H,^{15}N HSQC total correlation spectroscopy with 80-ms mixing time spectra were recorded.

The effects of complex formation on PCd were followed by acquiring two-dimensional ^{1}H,^{15}N HSQC spectra during titrations of aliquots of a 3.7 mM ferrous or 2.0 mM ferric C*f* solution into a solution of 0.2 mM ^{15}N-labeled PCd. The spectral widths were 32.0 ppm (^{15}N) and 12.0 ppm (^{1}H), and 256 and 1024 complex points were acquired in the indirect and direct dimensions, respectively. For measurements of the pseudo-contact shifts (PCS) ^{1}H,^{15}N HSQC spectra of free Pc, the oxidized complex and the reduced complex were acquired, always on the same sample. Ferric C*f* from a stock solution was added to a ^{15}N-labeled PCd sample with final concentrations of 0.35 and 0.50 mM, respectively. C*f* was reduced with 10 mol eq of a concentrated sodium ascorbate solution. Given the final C*f* concentration and the binding constant, the percentage of Pc bound was calculated to be 55%.

All data processing was performed with AZARA (www.bio.cam.ac.uk/azara), and analysis of the chemical-shift perturbations ($\Delta\delta_{Bind}$) with respect to the free protein was performed in Ansig (42–44). The spectra were calibrated against the internal standard [^{15}N]acetamide (0.5 mM).

Binding Curves—Titration curves were obtained by plotting $\Delta\delta_{Bind}$ against the molar ratio of $Cf^{II/III}$:PCd for the most strongly affected signals. Non-linear least squares fits to a 1:1 binding model (21) were performed in Origin 6.0 (Microcal Inc.). This model accounts for the dilution effect of both proteins during the titration, with the ratio of C*f* and PCd and $\Delta\delta_{Bind}$ as the independent and dependent variables, respectively. The binding constant (K_a) and the maximum chemical shift change ($\Delta\delta_{max}$) were the fitted parameters. A global fit of the data was performed in which the curves were fitted simultaneously to a single K_a value, whereas the $\Delta\delta_{max}$ for each resonance was allowed to vary.

Chemical Shift Mapping—The shifts observed in the complex PCd-Cf^{II} with 3 eq of C*f* were extrapolated to 100% bound for all residues using the K_a obtained from the fits. The average chemical-shift perturbation ($\Delta\delta_{avg}$) of each amide was calculated using the following equation (45),

$$\Delta\delta_{avg} = \sqrt{\frac{(\Delta\delta_N/5)^2 + \Delta\delta_H^2}{2}} \qquad \text{(Eq. 1)}$$

in which $\Delta\delta_N$ is the change in the ^{15}N chemical shift, and $\Delta\delta_N$ is the change in the ^{1}H chemical shift when the protein is 100% bound to C*f*.

Restraints Classes—Details of the restraints definitions are provided in the supplemental material. Briefly, four groups of restraints were defined. The interface restraints represent the chemical-shift perturbation data for Pc nuclei (Supplemental Table S1). These are satisfied when the nuclei are close the C*f* surface. Additional interface restraints were defined to serve as a weak van der Waals repel function. PCS were used to define pseudo-contact restraints and angle restraints according to the procedure described in Ubbink *et al.* (30), and minimal distance restraints were defined for amide groups that did not experience a PCS.

Electrostatic restraints based on kinetic rather than NMR data were used previously (30) to represent the electrostatic attraction between PCd and C*f*. In the *Nostoc* complex, these were not used because the NMR experimental data were sufficient to obtain a well defined structure.

A summary of the restraint groups is listed in Table I. The product between the number of restraints and the scaling factor used in the calculations indicates the importance of each restraint group. Note that the pseudo-contact restraints, which give quantitative information, are dominant.

Nostoc Cf Homology Model—A homology model of C*f* was built using the COMPOSER (46) module of SYBYL 6.5 (Tripos Inc.) using X-ray diffraction data from *Brassica rapa*, PDB entry 1CTM (resolution 2.30 Å (5)) and PDB entry 1HCZ (resolution 1.96 Å (47)) as templates. Including the structure of *Phormidium* C*f* (PDB entry 1CI3 (48)) as the template did not improve the model. Three sequence stretches (residues 1–9, 13–183, and 198–254) were considered as conserved. These regions

[2] C. Albarrán, J. A. Navarro, F. P. Molina-Heredia, P. del S. Murdoch, M. A. De la Rosa, and M. Hervás, submitted for publication.

TABLE I
Restraints groups

Restraint group	Type	Number of restraints	Scaling	Number × scaling
Interface	Distance	41	5	205
Pseudo-contact	Distance	81	20	1620
Minimal distance	Distance	90	10	900
Angle	Angle	81	[a]	

[a] Scaling of the angle restraints is not comparable with that of distance restraints.

showed identities of 66.7, 64.9, and 54.4%, respectively. Two loops corresponding to residues Trp-4—Gln-6 and Ala-184—Val-197 were simulated to allocate 1- and 3-residue insertions, respectively, using the TWEAK option. On average, the r.m.s.d. of backbone atoms of the model of C*f* with respect to the above structures was 0.56 Å. The structure of C*f* from *Mastigocladus* (made available only after completion of our calculations, PDB entry 1VF5 (6)) shows a similar extension of the small domain of C*f*. The *Nostoc* C*f* model shows a 1.16-Å r.m.s.d. with this structure. The largest differences correspond to residues 184–197, which show high B-factors in the *Mastigocladus* C*f* crystal structure, suggesting that this loop may be flexible.

Structure Calculations—Structure calculations were performed using XPLOR-NIH Version 2.9.1 (49, 50). The structures of *Nostoc* Pc (PDB entry 1NIN (40)) and the homology model of C*f* were treated as rigid bodies, and the co-ordinates of C*f* were fixed. PCd was placed at a random position and allowed to move in a restrained rigid-body molecular dynamics calculation. None of the standard energy terms was used. Only the groups of experimental restraints described above were applied to dock the proteins. Five thousand cycles (see supplemental material) of calculations were performed (9 h on a dual processor Pentium IV PC running under LINUX). Only structures with a total restraints "energy" (E_{tot}) below a threshold were saved, yielding ~90 structures. To assure sufficient sampling of the orientation space, a large random displacement of Pc occurred when a (local) minimum had been found, as judged from a total restrained energy that had not changed for more than 50% during 10 cycles. About 200 of such displacements occurred in a representative run. As an illustration, E_{tot} has been plotted against the cycle number in Fig. S2 for a sector of one trajectory, corresponding to 200 cycles.

The resulting structures were ranked according to total restraint energy and the top ten structures, with total restraint energy values from 28 to 29 arbitrary units subjected to restrained energy minimization of the side chains followed by a short restrained rigid body energy minimization, both using the XPLOR-NIH repulsive van der Waals term with reduced scaling. This largely removed the collisions between Pc and C*f* atoms while maintaining the low total restraint energy value. The ten best structures have been deposited in the Protein Data Bank under entry 1TU2. Buried surface areas have been calculated using NACESS (51).

Electron Transfer Pathways—To determine the residues that could be involved in the electron transport, the best electron transfer pathway for each of the energy-minimized complex structures was calculated using Greenpath Version 0.971 (52). This program performs a Green function analysis based on two-state super-exchange model (53). No enhanced coupling was used for aromatic rings. For representation purposes, we selected all the coordinates of the residues that appear in any of these paths instead of just representing the bonds and jumps involved.

RESULTS AND DISCUSSION

Binding Affinity—To characterize the complex of Pc and C*f* from *Nostoc*, C*f* was titrated into a solution of ^{15}N-labeled Cd-substituted Pc, PCd. The copper in Pc was replaced by the redox inactive substitute cadmium to allow for studies with both oxidized and reduced C*f* without interference from electron transfer reactions. The effects of the titrations were followed with two-dimensional HSQC experiments. Shifting of resonances during the titration indicated that binding and dissociation were fast on the NMR timescale (>100 s^{-1}). In Fig. 1, the chemical-shift perturbations due to binding to reduced C*f* (C*f*^{II}) are plotted for several residues of PCd. The curves clearly illustrate that the chemical-shift perturbations increase as a function of the C*f*^{II} concentration. A global fit of the data to a 1:1 binding model (21) yielded a binding constant of 16 ± 1 × 10^3 M^{-1}, and the same affinity was obtained with oxidized C*f* (K_A = 16 ± 2 × 10^3 M^{-1}; data not shown). This value is slightly lower than that obtained for native (Cu(I)) *Nostoc* Pc (26 ± 1 ×10^3 M^{-1} (64)). Hence, it can be concluded that the binding affinity is independent of the oxidation state of C*f* but appears to vary slightly between Pc with a singly charged metal and a doubly charged one.

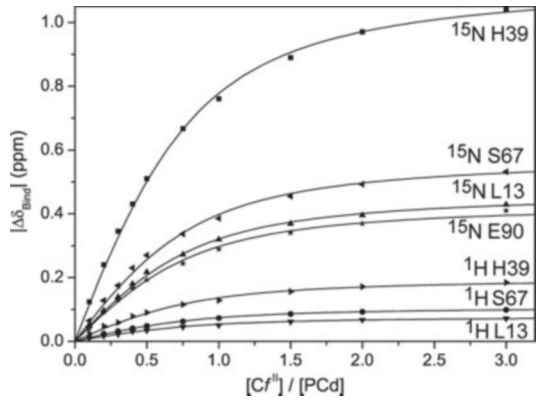

FIG. 1. **Binding curves for the interaction of *Nostoc* PCd in the presence of reduced C*f*.** $\Delta\delta_{Bind}$ is plotted against the ratio of C*f* and PCd. The data were fitted globally (non-linear, least squares) to a 1:1 binding model, yielding a binding constant of 16 ± 2 ×10^3 M^{-1}.

Interface Map—In Fig. 2, the size of the chemical-shift perturbations for residues affected upon titration with C*f*^{II} are color-coded onto the surface of Pc. Perturbed residues map in sequence stretches 7–17, 32–44, 63–72, and 88–100. These stretches form a large area comprising residues from both classical binding sites (10, 25). Three proline residues, at positions 37, 38, and 91 (*gray*), are located in the middle of the interface, close to the copper ligand His-92. In addition to the main interaction area, three isolated residues (Lys-51, Asp-54, and Leu-55) undergo a significant perturbation. These residues are located in a region below site 2, comprising mainly charged residues that have an important role in the *Nostoc* complex structure, as is explained below. The perturbation map of PCd is similar to that found for Pc(Cu(I)) (64).

The overall sizes of the perturbations and the localized nature of the binding map indicate that the complex between PCd and C*f* is well defined according to the classification for well defined *versus* dynamic complexes, suggested by Worrall *et al.* (55) and Prudêncio and Ubbink (56). That is, PCd adopts a single predominant conformation during most of the lifetime of the complex. This is also supported by the observation of intermolecular pseudo-contact effects, as explained below.

Experimental Restraints and Structure Calculation—When comparing the perturbations of Pc resonances observed with reduced and oxidized C*f*, it is striking that in the latter case many Pc nuclei experience an additional shift that is of similar size for ^{1}H and ^{15}N. This is illustrated in Fig. 3. The *top panel* shows the sizes of the perturbations of ^{1}H and ^{15}N for each Pc residue in the presence of reduced C*f*. It is clear that neither size nor sign correlate between the two types of nuclei. The *bottom panel* shows the additional shifts obtained when com-

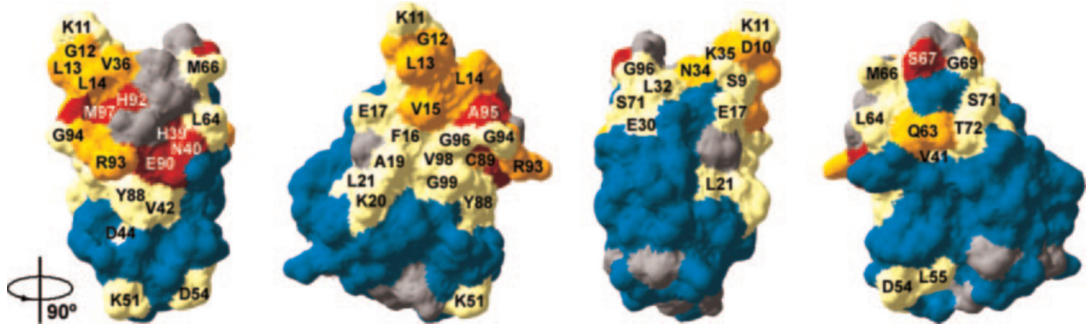

FIG. 2. **Chemical-shift perturbation map of *Nostoc* PCd in the presence of reduced C*f*.** Residues are colored according to their largest $\Delta\delta_{avg}$ (ppm): *blue* for <0.025, *white* for ≤0.050, *orange* for ≤0.100, *red* for ≤0.225. Prolines are indicated in *gray*. Residues are identified with the single-letter amino acid code, and the surfaces have been rotated 90° around the vertical axis for each picture, with respect to the one on the *left*. Surface representations were generated of the structure of *Nostoc* Pc (PDB entry 1NIN, model 1; 40) using Swiss-PdbViewer version 3.7 (54).

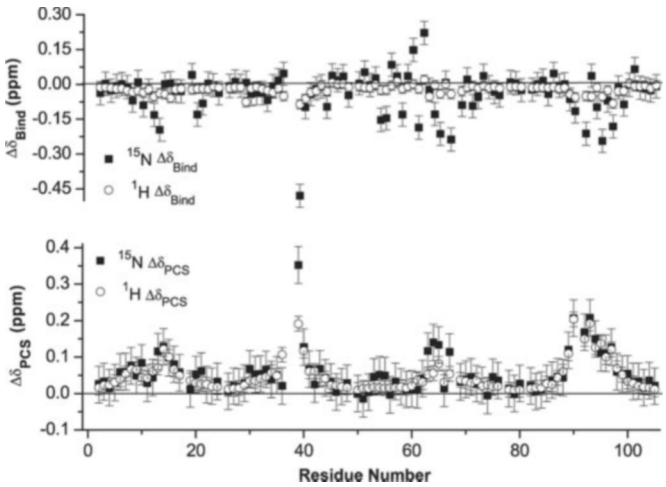

FIG. 3. **Chemical shift changes caused by binding effects (*upper panel*) and PCS (*lower panel*) are plotted for all residues of PCd.** The PCS were obtained as described in the supplemental material. The *error bars* represent the estimated experimental variation in chemical shift determination.

paring Pc in the presence of oxidized and reduced C*f* ($\Delta\delta_{oxidized}$-$\Delta\delta_{reduced}$). In this case there is a clear correlation of the shifts, suggesting that the additional shifts are caused by intermolecular PCS from the ferric heme iron onto Pc nuclei because these should be similar (in ppm) for the proton and nitrogen nuclei of a given amide. The strongest PCS are found in the hydrophobic patch region, suggesting that this region comes closest to the heme iron in the complex.

The binding effects and the PCS can be used to determine the orientation of Pc relative to C*f* in the complex. Both types of shifts were translated into restraints for a rigid-body docking calculation. The binding shifts were used in a qualitative manner; any shift larger than the threshold yields a restraint that requires that the amide is brought close to the surface of C*f* (interface restraints, Supplemental Table S1). The PCS are used quantitatively; during the calculations, the PCS are calculated for the given position of Pc and compared with the experimental values. If the difference is larger than the error margins, the restraint is violated. The position of Pc is changed, and the PCS are calculated again. Thus, in an iterative fashion, the optimal position, with minimal restraint violations is found. These are called the pseudo-contact restraints (Supplemental Table S1). The sign of the PCS gives information about the angle between iron-nucleus vector and the orientation of the magnetic susceptibility tensor, thus providing angle restraints. The absence of a PCS can be used to define a minimal-distance restraint, which is violated when the nucleus gets too close to the heme iron. Also, these restraints are evaluated iteratively during the calculations. All these restraints were used in a rigid-body calculation to obtain the orientation of Pc relative to C*f* with minimal violations of the experimental restraints. For this purpose the solution structure of Pc (40) and a homology model of C*f*, based on its conserved amino acid sequence, were used. Apart from the experimental restraint terms, no other forces, such as electrostatics, were used, except for a weak van der Waals repel function to avoid extensive collisions between the atoms of both proteins. Further details about the definitions and numbers of restraints as well as the calculations are given under "Experimental Procedures" and the Supplemental Material.

Results of the Structure Calculation—Two types of complexes were obtained from the above restrained rigid body calculations. All the structures with the lowest sum of violations (28.5 ± 0.5 arbitrary units) cluster in one orientation, with an average positional root mean square deviation of 1.3 ± 0.6 Å ("positional r.m.s.d."; see below), with respect to their average structure (Fig. 4). The iron-cadmium distance was 16.2 ± 0.1 Å. In addition, an alternative set of structures with another conformation was found (Supplemental Fig. S3). These have a higher sum of violations (38.9 ± 0.3 arbitrary units) and, thus, a much worse fit to the NMR data, in particular for the interface restraints, because the interaction surface is small and does not involve the hydrophobic patch. These structures have a significantly larger degree of variability with a positional r.m.s.d. of 3.2 Å and larger iron-cadmium distance (17.4 ± 0.1 Å). Consequently, these alternative complexes with larger violations, a small interface, and lower predicted efficiency in the electron transfer reaction are considered to be a non-physical solution of the calculations and are not considered further.

Quality of the Structure; Accuracy and Precision—The quality of the 10 best structures was evaluated on the basis of the violations between the calculated and the experimentally observed values for each group of restraints (see "Experimental Procedures"). With regard to interface restraints, systematic violations only appear for a few amide nuclei, with the largest found for Lys-20. The amides of these residues experience small chemical-shift perturbations upon binding that may be attributable to indirect effects (30). For the minimal distance restraints, there are a few small violations that correspond to Ile-101 in most of the 10 structures. This amino acid is at the boundary of residues that experience PCS.

The violations of the PCS restraints can be evaluated from Fig. 5*A*. The observed (*open symbols*) and predicted (*dashes* for the 10 best structures) PCS are plotted. For most residues, observed and predicted PCS agree within the error margins. However, some violations are observed, for Leu-13 (^{15}N), His-39 (^{15}N and ^{1}H), Asn-40 side chain (^{15}N and ^{1}H), Leu-65 (^{15}N), Glu-90 (^{1}H), His-92 (^{15}N and ^{1}H), and Arg-93 (^{1}H), with

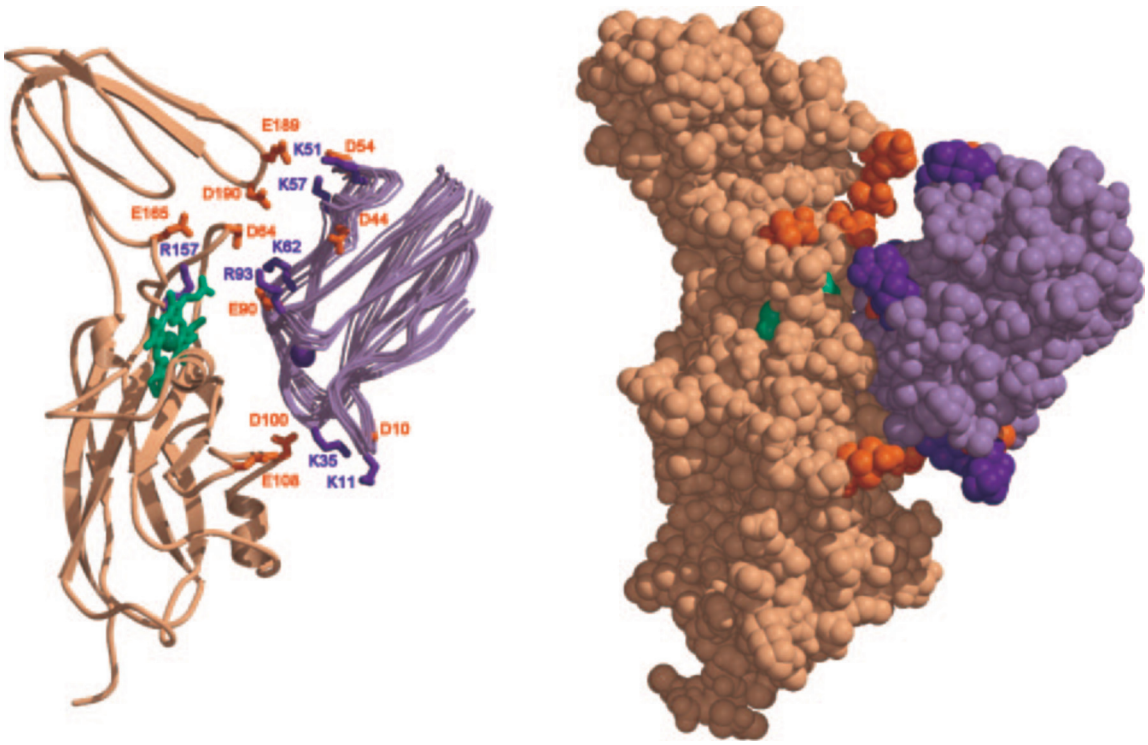

FIG. 4. **Structure of the *Nostoc* sp. PCC 7119 PCd-C*f* complex.** On the *left* the positions of the PCd backbone (C^{α} trace, in *blue*) relative to the C*f* (shown in *ribbons*) are shown for the 10 complexes with the lowest total of violations of the NMR-derived restraints. The average positional r.m.s.d. for the PCd structures compared with the mean is 1.3 ± 0.6 Å. The side chains of acidic amino acids are shown in *red*, whereas the basic residues are in *blue*. The heme group (represented in *sticks*) is colored in *green*, and the cadmium atom (shown as a *sphere*) is in *dark blue*. On the *right*, a space-filling representation is shown in the same orientation as on the *left*. Note the proximity of the hydrophobic and electrostatic surfaces on both proteins in the complex.

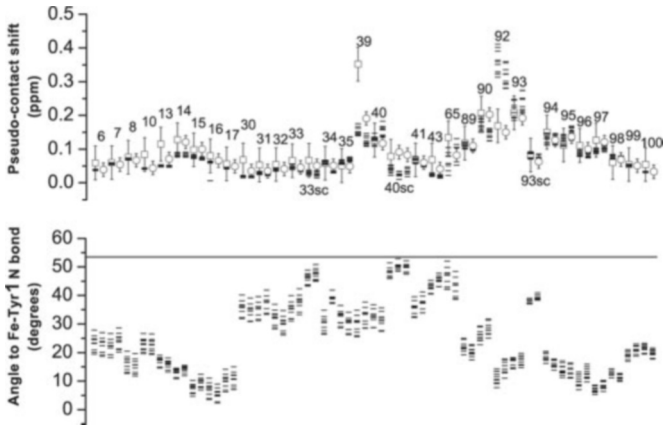

FIG. 5. **Violations for the Pc-C*f* complex.** The observed PCS are shown in the *top panel* with *open symbols* (*squares*, ^{15}N; *circles*, ^{1}H; *error bars* indicate estimated experimental errors in chemical shift determination). The *dashes* give the back-calculated values for the 10 best structures. Residue numbers are indicated; *sc*, side chain. In the *bottom panel*, the back-calculated angles between the nucleus that experiences a PCS, the heme iron, and Tyr-1 amino nitrogen atom are indicated with a *dash* for the same nuclei as in the *top panel*. Positive PCS should have angles <54° (*below* the *horizontal line*), and for negative PCS the angles should be >54°. It can be concluded that all angles in the calculated structures agree with the observed sign of the PCS.

the largest deviations for the two His residues, which are very close to the iron. It is likely that the necessary assumptions on the size, axiality, and orientation of the magnetic susceptibility tensor (see supplemental material) are the limiting factors in the accuracy of the structures. The angles between the assumed χ_{zz} direction and the iron-nucleus vector, as calculated from the ten best structures, are plotted in Fig. 5*B*. Positive PCS correspond to an angle smaller than 54°, and negative PCS have an angle larger than that. The angles observed in the structures are all in agreement with the positive sign of the PCS. The PCd position relative to that C*f* is the most relevant feature in the precision of the complex structure. After rigid-body and side-chain energy minimizations of the 10 structures, the positional r.m.s.d. is determined by aligning the C*f* molecules in each structure and calculating the r.m.s.d. of backbone heavy atoms of Pc compared with the average structure. The average backbone positional r.m.s.d. for PCd is 1.3 ± 0.6 Å for the 10 best structures. This precision is achieved without the input of electrostatic restraints in structure calculations as was done in the case of the complex of plant proteins (30) in which the positional r.m.s.d. was 1.05 Å. In the present case it can be concluded that the number of experimental restraints, which is larger than in previous studies, is sufficient to resolve a well defined structure.

Description of the Structure—The complex is shown in Fig. 4 in ribbon and space-filling representations. The binding interface involves the hydrophobic areas close to the metal centers in both proteins. In Pc it comprises 14 residues from the hydrophobic patch (Leu-14, Val-36, Pro-37, Pro-38, Leu-64, Met-66, Pro-68, Pro-91, His-92, and Ala-95), the neighboring Lys-35, and from the adjacent region of site 2 (Lys-62, Gln-63, and Glu-90). The buried area in this recognition patch on Pc is 572 $Å^2$. A second, minor recognition site on Pc corresponds to residues Asp-54 and Lys-57. It accounts for 41 $Å^2$ of the buried surface. This patch is clearly involved in electrostatic interactions with charged residues at the small domain region of C*f*. On C*f*, the recognition site measures 525 $Å^2$, comprising 20 residues that are at least partially buried during binding. Three of the five aromatic residues in this patch, namely Tyr-1, Phe-3, and Tyr-102, represent ~31% of the recognition surface of C*f*. Most residues at the recognition site are hydrophobic or polar, with charged residues lying at the rim of the interface.

Several aspects of the amino acid composition of the interface can be related to the transient nature of the complex. Charge interactions are observed at the edge of the interface, in accord with the general findings for transient complexes (33, 56). Residues Lys-57 and Lys-62 of Pc are close to Glu-189 and Asp-64 from C*f*, respectively. Several others (Asp-10, Lys-11, Lys-35, Asp-44, Lys-51, Asp-54, Asp-90, and Arg-93 from Pc and Asp-100, Glu-108, Glu-165, Asp-190 and the heme propionates in C*f*) are further away from the other protein but may be close enough to contribute to the electrostatic interactions. The charge interactions are expected to be favorable with negative charges on C*f* and predominantly positive ones on Pc.

Six proline residues are located in the interface, Pro-37, Pro-38, Pro-68, and Pro-91 from Pc and Pro-118 and Pro-120 from C*f* representing 17% of the residues at the interface and contributing ~30% to the buried surface area. Proline is a residue with very low propensity in protein-protein interfaces of tight complexes (3.8% (57–60)). However, proline is more abundant in transient protein complex interfaces (61). The inability of Pro to form hydrogen bonds may be employed in this way to limit the affinity in such complex. Four glutamine residues are found in the interface, representing 13.7% of the buried area (4.3% in recognition sites of tight complexes).

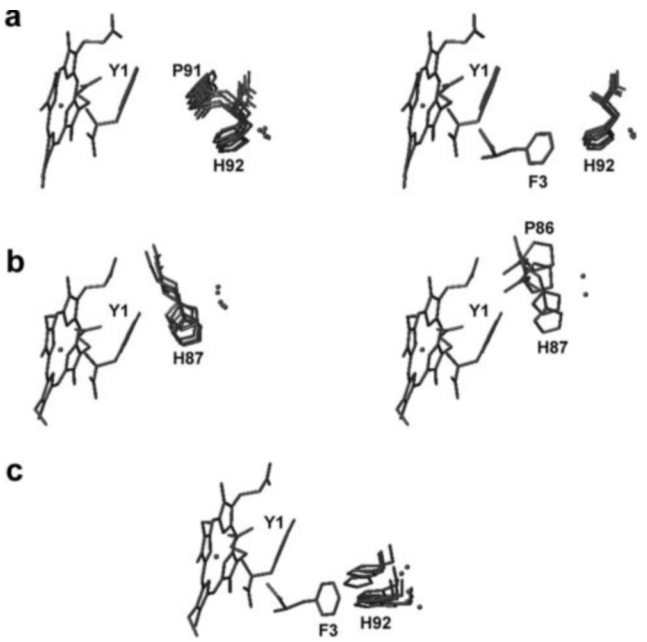

FIG. 6. **Important residues for electronic coupling for the ensemble of the 10 best conformations of Pc-C*f* complexes from *Nostoc* (*a*), plant (*b*) (30)), and *Phormidium* (*c*) (31)).** Diagrams show the copper atom of Pc, His-87 (His-92) copper ligand, Pro-86 (Pro-91), and the heme group with the distal ligand Tyr-1 and Phe-3 (in cyanobacterial C*f*). Residue numbers correspond to the organism represented in each panel. When two different pathways are found, the residues involved in the one with better coupling are represented on the *left*.

These polar, uncharged residues surrounding the hydrophobic patch may enhance dissociation by facilitating resolvation of the interface, as suggested previously by Crowley and Ubbink (33).

The buried surface area of the interface has a standard size for non-obligate protein complexes (57–60). Both sites (1 and 2) of Pc make contact with the C*f* surface, burying a total of 1100–1200 Å^2, similar to the 1200–1400 Å^2 in the *Phormidium* complex (31) and smaller than the 1720 Å^2 found in the plant complex (62).

Recent kinetic data using site-directed mutants of *Nostoc* Pc have revealed a large overlap between the recognition patches of Pc for PSI (63) and C*f*,[2] in particular for Pc substitutions affecting electrostatic interactions. However, there are some differences, according to the effects observed for several substitutions. For instance, Arg-93 mutants show a much larger effect on the electron transfer to PSI. Arg-93 belongs to the proximal patch of site 2, but it does not make contact with C*f* in the complex. The closest charged residue of C*f* (Glu-165) is 9 Å away. Thus, the electrostatic interaction between them may be moderate, and the kinetic effect of replacing Arg-93 could be attributable to more general electrostatic interactions, specifically during the encounter phase of the complex formation process, as described for the Arg-93 of *P. laminosum* Pc (28, 29). The mutation L14A has been shown to have a large effect on the reactivity of Pc toward PSI (63). On the other hand, this mutation has only minor effects (a 2-fold decrease in reaction rates) on the reduction of Pc by C*f*.[2] This is in agreement with the location of Leu-14 at the rim of the recognition site. Indeed, only a minor part (2 Å^2) of its solvent-accessible surface is buried in the complex interface.

Electronic Coupling—The structure reported herein is consistent with fast electron transfer. However, the average distance from iron to cadmium is the largest (16.2 ± 0.1 Å) found so far, with 11.0 and 13.9 Å in two plant complexes (30, 65) and 15.0 ± 2.0 Å for the complex of *Phormidium* (31).

To get information about the residues that may be involved in coupling of electron transfer between both proteins, the best theoretical paths in the ensemble of the energy-minimized structures of plant, *Phormidium*, and *Nostoc* were analyzed using Greenpath Version 0.971 (52). Putatively important residues are shown in Fig. 6. In all spinach structures Tyr-1 and His-87 (His-92 in *Nostoc*) are important for the electronic coupling, with a "path length" value (including bonds and through-space couplings) of 14.2 ± 0.4 Å. Similar results are found using the structure of the complex of poplar Pc with turnip C*f* complex (65), although in this case the path length is larger (19 ± 1 Å). In *Phormidium* the path length (19.4 ± 0.5 Å) is similar to that in poplar, but all the best pathways found involve the aromatic ring of Phe-3 in C*f*. In *Nostoc*, two sets of pathways are found in the final ensemble of structures; one (20.3 ± 0.8 Å) involving coupling via Tyr-1 in C*f* and Pro-91 and His-92 in Pc and another (22.2 ± 0.5 Å) via Phe-3 in C*f* and His-92 in Pc. The relative couplings for both pathways (3.6 ±

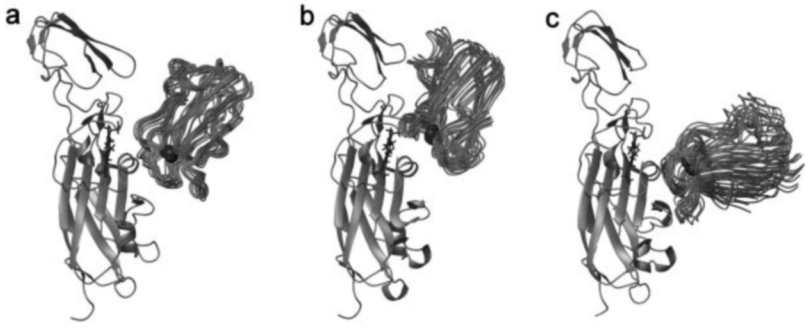

FIG. 7. **Comparison of the structures of PCd-C*f* complexes, showing the physiological cyanobacterial systems of *Nostoc* sp. PCC 7119 (*a*) and *P. laminosum* (*c*) and the conformation between poplar PCd and turnip C*f* (*b*).** C*f* is shown in *ribbons*, and Pc is represented by the ensemble of the 10 best conformations shown as C$^\alpha$ traces. The heme is in *sticks*, and the coppers are shown as *spheres*. Plant and *Nostoc* orientations show a side-on binding mode, whereas *Phormidium* exhibits a head-on conformation.

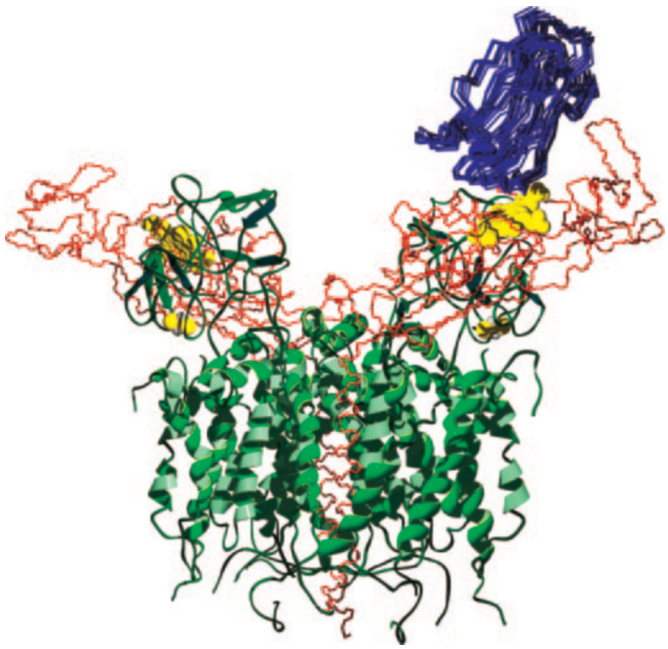

FIG. 8. **Model of the complex of plastocyanin and cytochrome b_6f.** The C*f* of the Pc-C*f* structures of *Nostoc* was aligned with one of the C*f* subunits of the cytochrome b_6f complex from *Mastigocladus* (PDB entry 1VF5 (6)). The cytochrome b_6f is shown in *green ribbons*, except for the C*f* subunits, which are shown as *backbone traces* in *red*. The 10 Pc models are shown as C^{α} traces. The C*f* heme groups, the Rieske iron-sulfur clusters, and the Pc copper ions are shown in space-filling representation.

0.6×10^{-9} and $1.6 \pm 0.3 \times 10^{-9}$) are somewhat smaller than those found for the plant and *Phormidium* structures ($5.3 \pm 0.8 \times 10^{-7}$ and $7 \pm 2 \times 10^{-8}$, respectively).

A combined Montecarlo and molecular dynamics calculation on a heterologous plant Pc-C*f* complex (17) suggested two electron pathways. The first involves Tyr-83 (in plant Pc). In all the solution structures reported including this one, the complex conformation is very different from that supporting this pathway (configuration E in Ref. 17). The *Nostoc* Pc residue equivalent to Tyr-83 (Tyr-88) is 12.5 Å away from the closest C*f* atom, and mutation of Tyr-88 to either Ala or Phe does not affect the reduction of Pc by C*f* in *Nostoc*.[2] The second pathway was described for the theoretical conformation D, which is the most similar to the *Nostoc* structure. It involves Pro-86 in plant Pc (Pro-91 in *Nostoc*) that should receive electrons from a C*f* heme propionate. The relative coupling for the theoretical complex (1.8×10^{-9}) is similar to those found for the *Nostoc* proteins. However, in the *Nostoc* structure the distance between Pro-91 and the heme is ~7 Å, too far for efficient direct electron transfer, and instead, the suggested pathway involves Tyr-1.

The Role of Electrostatic Interactions—Perhaps the most remarkable aspect of the *Nostoc* structure is the side-on binding of Pc. This conformation resembles the orientation found in the plant complex rather than the one found for the other cyanobacterial complex from *Phormidium* (Fig. 7). To establish the significance of the different orientations of Pc in the *Nostoc* and *Phormidium* complexes, the sum of violations was calculated for the *Nostoc* proteins, with Pc in the orientation of that found for *Phormidium*. The sum is significantly larger than those of the best structures, with larger minimum-distance and interface terms. The pseudo-contact restraints show a smaller violation for His-92, but the number of violations in the rest of the protein increases. To test whether this orientation corresponded to a local minimum in the conformational space, it was used as the input structure for a restrained rigid-body docking calculation. The calculation showed that Pc changed its orientation toward that of the 10 best structures (sum of violations, 30.8 arbitrary units; r.m.s.d. with the average of the 10 best structures, 1.5 ± 0.5 Å). It is concluded that the experimental data are sufficient to make a clear distinction between the different orientations.

The structure of the *Phormidium* complex does not exhibit a strong ionic strength dependence (31), and also the electron transfer kinetics show only a weak salt dependence (28, 29). Both the plant and the *Nostoc* complexes employ electrostatics but with reverse charges. In plant, positive charges on C*f* interact with the negative charges on Pc, whereas in *Nostoc* the opposite is observed. Such charge interactions are in accord with the kinetic studies. These have demonstrated a strong ionic strength dependence of the reduction reaction of Pc by C*f* *in vitro* for the plant system (21, 23–26, 28, 29), although the physiological significance of electrostatic interactions is not clear (15). Also for the *Nostoc* proteins the reaction is ionic strength-dependent.[2] Thus, it appears that a side-on binding of Pc is observed in complexes that involve electrostatic interactions. It is noteworthy that in the present calculations, electrostatic restraints were not used in any way (contrary to the plant case), and the present structure was based entirely on NMR spectroscopy-derived restraints.

It is also important to note that in all structures determined of Pc and C*f*, the orientation of Pc is such that a short electron transfer chain is created between the Q_o site of cytochrome b_6f and plastocyanin (involving the QH_2, Rieske FeS cluster, C*f* heme, and Pc copper). Fig. 8 shows a model of the cytochrome b_6f-Pc complex based on the structure of cytochrome b_6f (6) and the present structure of Pc-C*f*, obtained after alignment of the C*f* molecules. It is clear that C*f* faces the lumen with the region around heme ligand Tyr-1, readily forming a complex with Pc.

Acknowledgments—We are grateful to C. Albarrán for providing the plasmid of C*f* (pEAF-WT) and Drs. M. Hervás and J. A. Navarro for critical comments. Dr. M. Huber is acknowledged for help with the EPR spectroscopy.

REFERENCES

1. Blankenship, R. E. (2002) *Molecular Mechanisms of Photosynthesis*, Blackwell Science Ltd., Oxford
2. Allen, J. F. (2004) *Trends Plant Sci.* **9,** 130–137
3. Kallas, T. (1994) in *The Molecular Biology of Cyanobacteria* (Bryant, D. A., ed) pp. 259–317, Kluwer Academic Publishers Group, Dordrecht, Netherlands
4. Gray, J. C. (1992) *Photosynth. Res.* **34,** 359–374
5. Martinez, S. E., Huang, D., Szczepaniak, A., Cramer, W. A., and Smith, J. L (1994) *Structure* **2,** 95–105
6. Kurisu, G., Zhang, H. M., Smith, J. L., and Cramer, W. A. (2003) *Science* **302,** 1009–1014
7. Stroebel, D., Choquet, Y., Popot, J. L., and Picot, D. (2003) *Nature* **426,** 413–418
8. Sandmann, G., Reck, H., Kessler, E., and Böger, P. (1983) *Arch. Microbiol.* **134,** 23–27
9. Adman, E. T. (1991) *Adv. Protein Chem.* **42,** 145–197
10. Coleman, P. M., Guss, J. M., Sugimura, Y., Yoshizaki, F. Y., and Freeman, H. C. (1978) *J. Mol. Biol.* **211,** 617–632
11. Sykes, A. G. (1985) *Chem. Soc. Rev.* **14,** 283–321
12. Redinbo, M. R., Yeates, T. O., and Merchant, S. (1994) *J. Bioenerg. Biomembr.* **26,** 49–66
13. Bendall, D. S. (1996) in *Protein Electron Transfer* (Bendall, D. S. ed) pp.43–64, BIOS Scientific Publishers Ltd., Oxford
14. Pearson, D. C., Gross, E. L., and David, E. S. (1996) *Biophys. J.* **71,** 64–76
15. Soriano, G. M., Ponamarev, M. V., Tae, G. S., and Cramer, W. A. (1996) *Biochemistry* **35,** 14590–14598
16. Soriano, G. M., Cramer, W. A., and Krishtalik, L. I. (1996) *Biophys. J.* **73,** 3265–3276
17. Ullmann, G. M., Knapp, E. W., and Kostic, N. M. (1997) *J. Am. Chem. Soc.* **119,** 42–52
18. Pearson, D. C., and Gross, E. L. (1998) *Biophys. J.* **75,** 2698–2711
19. De Rienzo, F., Gabdouline, R. R., Menziani, M. C., Benedetti, P. G., and Wade, R. C. (2001) *Biophys. J.* **81,** 3090–3104
20. Gross, E. L., and Pearson, D. C. (2003) *Biophys. J.* **85,** 2055–2068
21. Kannt, A., Young, S., and Bendall, D. S. (1996) *Biochim. Biophys. Acta* **1277,** 115–126
22. Hope, A. B. (2000) *Biochim. Biophys. Acta* **1456,** 5–26
23. Soriano, G. M., Ponamarev, M. V., Piskorowski, R. A., and Cramer, W. A. (1998) *Biochemistry* **37,** 15120–15128
24. Gong, X. S., Wen, J. Q., Fisher, N. E., Young, S., Howe, C. J., Bendall, D. S.,

and Gray, J. C. (2000) *Eur. J. Biochem.* **267,** 3461–3468
25. Lee, B. H., Hibino, T., Takabe, T., Weisbeek, P. J., and Takabe, T. (1995) *J. Biochem.* **117,** 1209–1217
26. Illerhaus, J., Altschmied, L., Reichert, J., Zak, E., Herrmann, R. G., and Haehnel, W. (2000) *J. Biol. Chem.* **275,** 17590–17595
27. Gong, X. S., Went, J. Q., and Gray, J. C. (2000) *Eur. J. Biochem.* **267,** 1732–1742
28. Schlarb-Ridley, B. G., Bendall, D. S., and Howe, C. J. (2002) *Biochemistry* **41,** 3279–3285
29. Hart, S. E., Schlarb-Ridley, B., Delon, C., Bendall, D. S., and Howe, C. (2003) *Biochemistry* **42,** 4829–4836
30. Ubbink, M., Ejdebäck, M., Karlsson, B. G., and Bendall, D. S. (1998) *Structure* **6,** 323–335
31. Crowley, P. B., Otting, G., Schlarb-Ridley, B. G., Canters, G. W., and Ubbink, M. (2001) *J. Am. Chem. Soc.* **123,** 10444–10453
32. Crowley, P. B., Vintonenko, N., Bullerjahn, G. S., and Ubbink, M. (2002) *Biochemistry* **41,** 15698–15705
33. Crowley, P. B., and Ubbink, M. (2003) *Acc. Chem. Res.* **36,** 723–730
34. Crowley, P. B., Hunter, D. M., Sato, K., McFarlane, W., and Dennison, C. (2004) *Biochem. J.* **378,** 45–51
35. Castenholtz, R. W. (1970) *Schweiz. Z. Hydrol.* **32,** 538–551
36. Molina-Heredia, F. P., Hervás, M., Navarro, J. A., and De la Rosa, M. A. (1998) *Biochem. Biophys. Res. Commun.* **243,** 302–306
37. Ubbink, M., Lian, L. Y., Modi, S., Evans, P. A., and Bendall, D. S. (1996) *Eur. J. Biochem.* **242,** 132–147
38. Schulz, H., Fabianeck, R. A., Pellicioli, E. C., Hennecke, H., and Thöny-Meyer, L. (1999) *Proc. Natl. Acad. Sci. U. S. A.* **96,** 6462–6467
39. Ubbink, M., Van Beeumen, J., and Canters, G. W. (1992) *J. Bacteriol.* **174,** 3707–3714
40. Badsberg U., Jorgensen A. M., Gesmar H., Led J. J., Hammerstad J. M., Jespersen L. L., and Ulstrup J. (1996) *Biochemistry* **35,** 7021–7031
41. Andersson, P., Gsell, B., Wipf, B., Senn, H., and Otting, G. (1998) *J. Biomol. NMR* **11,** 279–288
42. Kraulis, P. J. (1989) *J. Magn. Reson.* **84,** 627–633
43. Kraulis, P. J., Domaille, P. J., Campbell-Burk, S. L., van Aken, T., and Laue, E. D. (1994) *Biochemistry* **33,** 3515–3531
44. Helgstrand, M., Kraulis, P., Allard, P., and Hard, T. (2000) *J. Biomol. NMR* **18,** 329–336
45. Grzesiek, S., Bax, A., Clore, G. M., Gronenborn, A. M., Hu, J. S., Kaufman, J., Palmer, I., Stahl, S. J., and Wingfield, P. T. (1996) *Nat. Struct. Biol.* **3,** 340–345
46. Blundell, T., Carney, D., Gardner, S., Hayes, F., Howlin, B., Hubbard, T., Overlington, J., Singh, D. A., Sibanda, B. L., and Sutclife, M. (1988) *Eur. J. Biochem.* **172,** 513–520
47. Martinez, S. E., Huang, D., Ponomarev, M., Cramer, W. A., and Smith, J. L. (1996) *Protein Sci.* **5,** 1081–1092
48. Carrell, C. J., Scharlb, B. G., Bendall, D. S., Howe, C. J., Cramer, W. A., and Smith, J. L. (1999) *Biochemistry* **38,** 9590–9599
49. Brunger, A. T. (1992) *X-PLOR 3.1 Manual*, Yale University Press, New Haven, Connecticut
50. Schwieters, C. D., Kuszewski, J. J., Tjandra, N., and Clore, G. M. (2003) *J. Magn. Reson.* **160,** 66–74
51. Hubbard, S. J., Campbell, S. F., and Thornton, J. M. (1991) *J. Mol. Biol.* **220,** 507–530
52. Regan, J. J. (1994) *Greenpath software*, Version 0.9771, San Diego, CA
53. Skourtis, S. S., and Onuchic, J. N. (1993) *Chem. Phys. Lett.* **209,** 171–177
54. Guex, N, and Peitsch, M. C. (1997) *Electrophoresis* **18,** 2714–2723
55. Worrall, J. A. R., Liu, Y. J., Crowley, P. B., Nocek, J. M., Hoffman, B. M. and, Ubbink, M. (2002) *Biochemistry* **41,** 11721–11730
56. Prudêncio, M., and Ubbink, M. (2004) *J. Mol. Recognit.* **17,** 524–539
57. Jones, S., and Thornton, J. M. (1996) *Proc. Natl. Acad. Sci. U. S. A.* **93,** 13–20
58. Jones, S., and Thornton, J. M. (1997) *J. Mol. Biol.* **272,** 121–132
59. Chakrabarti, P., and Janin, J. (2002) *Proteins Struct. Funct. Genet.* **47,** 334–343
60. Wodak, S. J., and Janin, J. (2003) *Adv. Protein Chem.* **61,** 9–73
61. Crowley, P. B., and Carrondo, M. A. (2004) *Proteins* **55,** 603–612
62. Ubbink, M. (2001) in *Handbook of Metalloproteins* (Messerschmidt, A., Huber, R., Poulos, T., and Wieghardt, K., ed) pp. 182–192, John Wiley & Sons, Inc., Chichester, UK
63. Molina-Heredia, F. P., Hervás, M., Navarro, J. A., and De la Rosa, M. A. (2001) *J. Biol. Chem.* **276,** 601–605
64. Díaz-Moreno, I. Díaz-Quintana, A. De la Rosa, M. A. Crowley P. B., and Ubbink, M. (2005) *Biochemistry* **44,** 3176–3183
65. Lange, C. Cornvik, T. Díaz-Moreno I., and Ubbink, M. (2005) *Bioenergetics*, in press